

# On the Application of Support Vector Machines to the Prediction of Propagation Losses at 169 MHz for Smart Metering Applications

Martino Uccellari, Francesca Facchini, Matteo Sola, *Member, IEEE*, Emilio Sirignano, Giorgio M. Vitetta, *Senior Member, IEEE*, Andrea Barbieri and Stefano Tondelli

**Abstract**—Recently, the need of deploying new wireless networks for smart gas metering has raised the problem of radio planning in the 169 MHz band. Unluckily, software tools commonly adopted for radio planning in cellular communication systems cannot be employed to solve this problem because of the substantially lower transmission frequencies characterizing this application. In this manuscript a novel data-centric solution, based on the use of support vector machine techniques for classification and regression, is proposed. Our method requires the availability of a limited set of received signal strength measurements and the knowledge of a three-dimensional map of the propagation environment of interest, and generates both an estimate of the coverage area and a prediction of the field strength within it. Numerical results referring to different Italian villages and cities evidence that our method is able to achieve good accuracy at the price of an acceptable computational cost and of a limited effort for the acquisition of measurements in the considered environments.

**Index Terms**—Machine learning, support vector machine, measurement, received signal strength, radio coverage, smart metering, open data.

## I. INTRODUCTION

In recent years an increasing attention has been paid to the development of advanced systems for electricity, gas and water metering. Various *advanced metering infrastructure* (AMI) solutions are currently available on the market. All of them are based on a hierarchical topology, in which multiple indoor *smart meters* are connected to a *gateway* (also called *data collector* or *concentrator*), which collects their measurements and send them to an infrastructure where the acquired data are stored and processed. Recently, the *Open Metering System* group has proposed the adoption of the *Wireless M-Bus* technology for metering scenarios and, in particular, has recommended its use in smart meters [1], [2], because of its low energy requirements and its use of sub-GHz transmission bands for long range communications. Note that, whereas ref. [1] prescribed the use of the 868 MHz and

468 MHz bands, ref. [2] has added new transmission modes providing lower data rates in the 169 MHz band, which has been recently relocated by the European Union to specific applications for smart metering [3]. Since outdoor radio-wave propagation is easier at lower frequencies, the 169-MHz band is currently adopted for automated meter-reading purposes in various European countries (e.g. in Italy, France, and Spain). In particular, point to multipoint networks operating in the 169 MHz band have been proposed for the Italian gas market by the *Italian Gas Committee* (CIG). The design of new AMIs for gas resources in that band has unavoidably raised the important problem of radio planning at 169 MHz; in fact, this problem cannot be solved by means of the software tools devised for cellular networks because of the substantially higher transmission frequencies employed in such networks. Moreover, the development of new tools requires an in-depth understanding of the propagation losses experienced over the wireless links connecting data concentrators and smart meters. Unluckily, few results are available in the technical literature about such losses in the 169 MHz band and the available prediction methods for those frequencies may not provide a unique outcome. Recently, the problem of assessing the propagation losses at 169 MHz has been investigated by [4] for its practical relevance. The interesting results illustrated in that manuscript refer, however, to the *outdoor-to-indoor* propagation losses only (in particular, to the so called *building penetration losses*), that is to the main signal attenuation produced by the obstruction of the walls of the building in which a given smart meter is installed; unluckily, no result is provided about the *prediction of outdoor propagation losses*, i.e. about the mean attenuation that would be experienced over a given link at a arbitrary distance if the involved smart meter was placed outdoor. In this manuscript we tackle the last problem and develop a novel solution to the problem of predicting outdoor propagation losses at 169 MHz.

It is well known that, generally speaking, the prediction of wireless path losses can be based on *a priori models* or on *models based on a set of measurements acquired in various locations of that scenario* [5]. The models of the first category allow engineers to make predictions exploiting available prior knowledge only, without making use of explicit measurements; these include various models based on different analytical methods (and, possibly, including corrections factors deriving from measurements acquired in one or more environments,

Martino Uccellari, Matteo Sola, Emilio Sirignano and Giorgio M. Vitetta are with the Department of Engineering “Enzo Ferrari”, University of Modena and Reggio Emilia, Modena, Italy (e-mail: matteo.sola@unimore.it, emilio.sirignano@unimore.it, giorgio.vitetta@unimore.it). Francesca Facchini is with the University of Modena and Reggio Emilia, where she is enrolled in an industrial PhD program supported by the company CPL Concordia (Concordia, Modena, Italy; e-mail: francesca.facchini@unimore.it). Andrea Barbieri and Stefano Tondelli are with the company CPL Concordia, that has funded this work under the contract “Wireless channel modelling in the 169 MHz band”.

like the well known *Hata-Okumura model* [6], [7]) and the so called *ray-tracing models* [8]. These models are most appropriate for making predictions when it is impossible or difficult to obtain measurements and are characterized by different degrees of accuracy, knowledge of propagation environment and complexity (for instance, ray-tracing models may offer accurate predictions at the price of their large computation and data requirements). On the contrary, the second category is based on a data-centric approach known as *modelling with measurements* [5]; the models it includes rely on the idea that that there is no single set of a priori constants, functions, or data able to provide an accurate description of a new propagation environment. For this reason, the evaluation of reliable predictions requires collecting measurements at multiple locations and fitting them to estimate propagation losses at different locations. Note that this approach can result in truthful predictions at the price of a moderate effort in data acquisition and of an acceptable computational load; consequently, it may provide useful solutions for practical applications. Unluckily, a limited number of papers about this category of models is available in the technical literature (see [5] and references therein) and, as far as we know, none of them addresses the problem of predicting the propagation losses in the 169 MHz band. This has motivated our interest in developing a specific methodology for solving this problem. The approach we adopted in our work has been inspired by some previous work on the application of *machine learning techniques* [9] and, in particular, of *supervised learning algorithms* to the problem of field strength prediction (e.g., see [10]–[16]) and is based on the use of: a) a nonlinear model for representing, respectively, the *received signal strength* (RSS) measurements collected at ground level in multiple locations of a given scenario; b) a significant (but small) set of *features* depending on the type of scenario in which RSS is predicted and extracted from a *three-dimensional* (3D) geometrical representation of the considered propagation environment; c) *support vector machine* (SVM) algorithms to estimate the system coverage area and predict the dependence of RSS on receiver location inside the coverage area itself. The proposed method can be easily implemented using public SVM libraries, requires the use of low cost commercial hardware for data acquisition, and entails an acceptable computational load for the considered application; moreover, as evidenced by our numerical results, it is able to provide accurate predictions in different propagation scenarios. For this reason, we believe that it represents the key for the development of efficient software tools for radio planning of AMIs operating at 169 MHz.

It is important to mention that the application of SVM methods to the field strength prediction is not new and that, in particular, has been previously investigated in [10], [16] and [18]. However, our contribution represents a significant advancement with respect to previous work since: a) the numerical results illustrated in those manuscripts refer to substantially higher frequencies (900 MHz, 947 MHz and 853.71 MHz, respectively); b) each of those manuscripts refers to a single urban scenario, whereas various propagation environments have been taken into consideration in assessing the performance of our method; c) the set of features taken

into consideration in our work differs from that adopted in previous works and is small (so that the use of *dimensionality reduction techniques*, like those considered in [16], is not required); d) unlike the technical solutions proposed in those manuscripts, our approach combines SVM-based *classification* and *regression* algorithms in field strength prediction; e) unlike [10], our results are entirely based on real measurements.

The remaining part of this manuscript is organized as follows. In Section II the prediction of propagation losses in the 169 MHz band is formulated as a nonlinear regression problem and a specific solution based on the use of SVM-based classification and regression techniques is illustrated. A description of the environments considered in our measurement campaigns and of the measurement tools adopted in the acquisition of RSS data is provided in Section III. In Section IV we analyse the set of features we selected for RSS prediction and provide various details about the implementation of the specific software tool we developed for radio planning. Various numerical results are illustrated and commented in Section V. Finally, some conclusions are offered in Section VI.

## II. SUPPORT VECTOR MACHINES FOR THE PREDICTION OF THE PROPAGATION LOSSES

In this Section we first formulate the problem of field strength prediction in a specific environment. Then, we propose a specific solution based on SVM methods for classification and regression.

### A. Problem statement

Following [4], the total propagation loss affecting the wireless link between an indoor gas meter and a data concentrator can be expressed (in dB) as

$$L_{TOT} = \langle PL \rangle + X_{SH} + X_{BPL} + \langle IL \rangle, \quad (1)$$

where  $\langle PL \rangle$  is the *path loss* (i.e., the mean attenuation that would be experienced over the given link at the same distance if the meter was placed outdoor), whereas  $X_{SH}$ ,  $X_{BPL}$  and  $\langle IL \rangle$  represent the *outdoor shadowing*, the *building penetration loss* (BPL) and the mean *installation loss* (IL; this term is due to the additional signal shielding that originates from meter housing), respectively. Specific indications about the modelling of  $X_{BPL}$  and  $\langle IL \rangle$  are provided in [4]; for this reason, in our work we focus on the problem of predicting the quantity

$$L_P = \langle PL \rangle + X_{SH}, \quad (2)$$

that represents the so called *outdoor propagation loss*. Note that, if  $L_P$ ,  $X_{BPL}$  and  $\langle IL \rangle$  were known, the link budget equation

$$P_{RX} = P_{TX} + G_{TX} + G_{RX} - L_P - X_{BPL} - \langle IL \rangle, \quad (3)$$

could be used to assess the field strength at an arbitrary distance and, consequently, to assess the *system coverage area* (i.e., the geographical area served by the considered concentrator); here,  $P_{RX}$  ( $P_{TX}$ ) and  $G_{TX}$  ( $G_{RX}$ ) denote the receive (transmit) power<sup>1</sup> (expressed in dBm) and the

<sup>1</sup>Received power should be always interpreted as a *local mean*, since multipath fading effects are averaged out in our measurement procedure.

transmit (receive) antenna gain (expressed in dB), respectively. However, in the following, since we are interested in  $L_P$  (2), and  $P_{TX}$ ,  $G_{TX}$  and  $G_{RX}$  are perfectly known, we take into consideration the specific problem of predicting  $P_{RX}$  in an outdoor scenario. For this reason, in this case, the link budget equation

$$P_{RX} = P_{TX} + G_{TX} + G_{RX} - L_P \quad (4)$$

should be employed in place of (3). It is also worth mentioning that: a) the sum  $G_{TX} + G_{RX}$  is quite small in the considered scenario since a low efficiency should be expected for the antenna at the meter side; b) estimating the system coverage area means delimiting the area that surrounds the considered concentrator and such that, if a given meter is placed inside it, the inequality

$$P_{RX} \geq P_{RX-SENS} \quad (5)$$

holds, where  $P_{RX-SENS}$  is the *receiver sensitivity threshold* ( $P_{RX-SENS} = -119 \text{ dBm}$  in this case); from the last expression and (4) it is easily inferred that, from a mathematical viewpoint, this is equivalent to delimiting the area in which the propagation loss  $L_P$  satisfies the inequality

$$L_P \leq -P_{RX-SENS} + P_{TX} + G_{TX} + G_{RX}. \quad (6)$$

In our work the estimation of the coverage area and the prediction of the field strength within it are based on the following data:

- 1) A 3D geometrical representation of the considered propagation environment. As it will become clearer later, the required representation is provided by typical topographic maps in digital format; in fact, these usually contain essential information about building size and position, and about contours connecting points at the same elevation<sup>2</sup> (if the considered area is hilly or mountainous); as it will become clearer later, these information are needed for the computation of specific position-dependent *features*, whose knowledge is required by the developed SVM-based algorithms for all the locations at which measurement have been collected and field strength is predicted. Note also that typical maps usually provide various information about roads; such information may be required in our approach, but not for the evaluation of the above mentioned features. In fact, as it will be explained in more detail in Paragraph IV-C, road information can be exploited in some cases to improve the quality of position estimates provided by the *global positioning system* (GPS) receiver embedded in our measurement hardware.
- 2) A set  $\{m_i; i = 1, 2, \dots, N\}$  collecting  $N$  power measurements acquired at  $N$  distinct locations of the considered environment (the experimental set-up adopted in our measurement campaign is described in detail in Paragraph III-A).

In our work the nonlinear model

$$m_i = f(\mathbf{x}_i) + n_i \quad (7)$$

<sup>2</sup>Vector maps available in topographic databases usually contain the required information.

is adopted for the  $i$ -th measurement (with  $i = 1, 2, \dots, N$ ); here, the function  $f(\cdot)$  expresses the *nonlinear* dependence of the considered power on a  $m$ -dimensional vector  $\mathbf{x}_i = [x_i^{(1)}, x_i^{(2)}, \dots, x_i^{(m)}]^T$  collecting  $m$  distinct features<sup>3</sup> and  $n_i$  is the additive noise affecting the  $i$ -th measurement (noise is mainly due to the measurement equipment and to the non ideal spatial averaging of the received power, and is assumed to be statistically independent of the position  $\mathbf{p} = [x, y, z]^T$  at which data are acquired). As it will become clearer later, the selected features depend on the coordinate vector  $\mathbf{p}_i = [x_i, y_i, z_i]^T$  identifying the  $i$ -th measurement location (in practice, an estimate  $\tilde{\mathbf{p}}_i = [\tilde{x}_i, \tilde{y}_i, \tilde{z}_i]^T$ , generated by a GPS device, is available for this vector) and on various characteristics of the propagation environment (including the transmitter location), as illustrated in detail in Paragraph IV-A. It is also important to keep in mind that any meaningful power measurement is lower bounded by the receiver sensitivity (in other words,  $m_i \geq P_{RX-SENS}$  inside the coverage area) and that the conventional value  $P_{NC} = -120 \text{ dBm}$  is assigned to all the measurements acquired at the positions in which the transmitted signal is not correctly received or is not received at all (in other words, outside the coverage area).

Given the information and the measurement models illustrated above, we are interested in developing a procedure for solving the following two correlated problems: a) identifying the system coverage area; b) evaluating an approximate expression of the function  $f(\cdot)$  appearing in (7), so that a field strength map (or, equivalently, a propagation loss map) can be generated. Note that, on the one hand, the first problem can be interpreted as a *binary classification problem*, since it concerns differentiating the cases in which a reliable wireless link can be established from those in which this is impossible. On the other hand, the second one can be seen as a *nonlinear regression problem* [9], since it concerns the prediction of the field strength at positions different from those for which measurements are available. In the following Paragraph we show that both problems can be tackled resorting to SVM techniques and that the solution to the first problem provides some useful information that can be exploited in the second problem.

### B. Application of Support Vector Machines to the Prediction of System Coverage and Field Strength

As already mentioned above, the first part of our approach concerns the identification of the system coverage area; this problem can be formulated as a binary classification problem. In fact, the available information, represented by the data set  $S^{(m)} \triangleq \{(\mathbf{x}_i, m_i), i = 1, 2, \dots, N\}$ , can be employed to generate the new set  $S^{(z)} \triangleq \{(\mathbf{x}_i, z_i), i = 1, 2, \dots, N\}$ , where  $z_i$  represents a binary *categorical attribute* (or *class label*) specifying the absence or presence of radio coverage at the location  $\mathbf{x}_i$  and taking on the values  $\{\pm 1\}$  only; in particular  $z_i = +1$  ( $z_i = -1$ ) identifies the presence (lack)

<sup>3</sup>Generally speaking, the set of features should include all the geometrical and physical parameters that may significantly influence field strength at an arbitrary position; the specific features we have selected for our measurement model (7) are defined in Paragraph IV-A.

of radio coverage and is associated with  $m_i \geq P_{RX-SENS}$  ( $m_i = P_{NC}$ ), since the received signal strength is (not) large enough to ensure a reliable reception. In our approach, the set  $S^{(z)}$  is partitioned into the *training set*  $S_{train}^{(z)} \triangleq \{(\mathbf{x}_i, z_i), i = 1, 2, \dots, N_{train}^{(z)}\}$  and in the *test set*  $S_{test}^{(z)} \triangleq \{(\mathbf{x}_i, z_i), i = N_{train}^{(z)} + 1, N_{train}^{(z)} + 2, \dots, N_{train}^{(z)} + N_{test}^{(z)}\}$ , consisting of  $N_{test}^{(z)}$  and  $N_{train}^{(z)} \triangleq N - N_{test}^{(z)}$  points, respectively. Then, the set  $S_{train}^{(z)}$  is processed by a *C - support vector classification* (C-SVC) algorithm [19], [20], that aims at identifying an *hyperplane*  $H$  (in a proper  $d$ -dimensional Euclidean space  $\mathcal{H}$ ) separating the positive examples (i.e., those associated with a categorical attribute equal to +1) from the negative ones (i.e., those corresponding to a categorical attribute equal to -1), while keeping the *hyperplane margin* (i.e., the hyperplane distance from the closest positive and negative examples) as large as possible and the number of classification errors<sup>4</sup> in the training process as small as possible; note that, generally speaking, the points of  $H$  satisfy the equation

$$\mathbf{w} \cdot \phi(\mathbf{x}) + b = 0, \quad (8)$$

where  $\phi(\mathbf{x})$  represents a proper mapping<sup>5</sup> of  $\mathbf{x}$  into the space  $\mathcal{H}$ ,  $\mathbf{w} = [w_1, w_2, \dots, w_d]^T$  denotes a  $d$ -dimensional real vector normal to  $H$  and  $b$  is a real parameter such that  $|b| / \|\mathbf{w}\|$  is the perpendicular distance of the origin from  $H$  (here the operators  $\cdot$  and  $\|\cdot\|$  denote the scalar product between two vectors and the Euclidean norm of a vector, respectively). In practice, the problem of finding  $H$  can be formulated as the (*primal*) optimization problem

$$\min_{\mathbf{w}, b, \xi} \frac{1}{2} \mathbf{w}^T \mathbf{w} + C \sum_{i=1}^{N_{train}^{(z)}} \xi_i \quad (9)$$

subject to the constraints

$$\xi_i > 0 \quad (10)$$

and

$$z_i [\mathbf{w}^T \phi(\mathbf{x}_i) + b] \geq 1 - \xi_i, \quad (11)$$

with  $i = 1, 2, \dots, N_{train}^{(z)}$ . Here,  $\xi_i$  is the  $i$ -th *slack variable* (the slack variables are collected in the vector  $\xi \triangleq [\xi_1, \xi_2, \dots, \xi_{N_{train}^{(z)}}]^T$ ) and  $C$  is a *regularization parameter* to be chosen by the user. It is important to point out that: a) the slack variables are included in the considered problem to account for the presence of the above mentioned classification errors (in practice, the occurrence of a specific error is associated with the corresponding slack variable exceeding unity, so that the sum  $\sum_{i=1}^{N_{train}^{(z)}} \xi_i$  appearing in (9) represents an upper bound on the overall number of these errors); b) consequently, the parameter  $C$  allows the SVM user to control the weight of these errors in the objective function of (9). The constrained optimization problem (9)-(11) can be easily reformulated as a

<sup>4</sup>Errors are due to the fact that, generally speaking, in the considered problem the data collected in  $S^{(y)}$  are *not separable*, i.e. an hyperplane separating the points with opposite categorical attributes does not exist.

<sup>5</sup>As it will become clearer later, we do not need to give an explicit expression for this function.

*Lagrangian problem*; it is not difficult to prove that this leads to the *dual problem*

$$\min_{\alpha} \frac{1}{2} \alpha^T \mathbf{Q} \alpha - \mathbf{e}^T \alpha \quad (12)$$

subject to

$$\mathbf{z}^T \alpha = 0 \quad (13)$$

and

$$0 \leq \alpha_i \leq C, \quad (14)$$

with  $i = 1, 2, \dots, N_{train}^{(z)}$ . Here,  $\mathbf{z} \triangleq [z_1, z_2, \dots, z_{N_{train}^{(z)}}]^T$ ,  $\alpha \triangleq [\alpha_1, \alpha_2, \dots, \alpha_{N_{train}^{(z)}}]^T$  is the vector collecting the (positive) Lagrange multipliers,  $\mathbf{e} = [1, 1, \dots, 1]^T$  is the  $N_{train}^{(z)}$ -dimensional vector of all ones,  $\mathbf{Q} = [Q_{i,j}]$  is a  $N_{train}^{(z)} \times N_{train}^{(z)}$  positive semidefinite matrix with  $Q_{i,j} = z_i z_j K(\mathbf{x}_i, \mathbf{x}_j)$  and  $K(\mathbf{x}, \hat{\mathbf{x}}) \triangleq \phi^T(\mathbf{x}) \phi(\hat{\mathbf{x}})$  is the so called *kernel function*, which, as it will become clearer in Paragraph IV-B, contains a single parameter (denoted  $\gamma$ ) to be optimized. Solving the convex quadratic optimization problem (12)-(14) yields the vector  $\alpha_o = [\alpha_{o,1}, \alpha_{o,2}, \dots, \alpha_{o,l}]^T$  of Lagrange multipliers, from which the optimal value

$$\mathbf{w}_o = \sum_{i=1}^{N_{train}^{(z)}} z_i \alpha_{o,i} \phi(\mathbf{x}_i) \quad (15)$$

of  $\mathbf{w}$  and the optimal value  $b_0$  of  $b$  can be evaluated. Given  $\mathbf{w}_o$  and  $b_0$ , the *decision function*

$$\begin{aligned} d(\mathbf{x}) &\triangleq \text{sgn}(\mathbf{w}_o^T \phi(\mathbf{x}) + b_o) \\ &= \text{sgn}\left(\sum_{i=1}^{N_{train}^{(z)}} z_i \alpha_{o,i} K(\mathbf{x}_i, \mathbf{x}) + b_o\right), \end{aligned} \quad (16)$$

can be computed. This function is employed to classify an arbitrary feature vector  $\mathbf{x}$  not included in the training set; in fact, in the considered problem this vector is assigned (not assigned) to the coverage area if  $d(\mathbf{x}) = 1$  ( $d(\mathbf{x}) = -1$ ). In particular, the function  $d(\mathbf{x})$  (16) can be evaluated for all the locations which the test set  $S_{test}^{(z)}$  refers to in order to assess the classification accuracy. Note that this accuracy is unavoidably influenced by the two parameters  $C$  and  $\gamma$  appearing in the objective function of (9) and in the kernel function, respectively. For this reason, a *cross-validation* procedure is usually needed to adjust these parameters for optimizing classification performance (e.g., see [21, Par. 3.2] for a detailed analysis of this problem), as will be discussed in some detail in Paragraph V-A.

The classification procedure described above deserves also the following comments:

- 1) In generating the set  $S^{(y)}$ , the experimental data collected in a specific measurement campaign undergo a pseudorandom permutation in order to avoid that the data collected in  $S_{train}^{(z)}$  and those included in  $S_{test}^{(z)}$  refer to disjoint portions of the area in which such measurements have been collected. Ignoring this simple rule might entail a significant loss in the *generalization capability* of our classification and regression methods.
- 2) In our work, unless explicitly stated, the training set  $S_{train}^{(z)}$  contains eighty percent of the data collected in  $S^{(z)}$ .

- 3) As it will become clearer later, the decision function  $d(\mathbf{x})$  (16) can be exploited in the regression procedure described below.

The other part of our approach is represented by a regression procedure which generates a prediction of the RSS map inside the coverage area. From a mathematical viewpoint, such a procedure generates an hyperplane in the space of features; however, generally speaking, this hyperplane is different from that produced by our classification method and is employed for predicting the field strength at unknown locations. Similarly as the classification procedure, the adopted procedure requires a *training set*  $S_{train}^{(m)}$  and a *test set*  $S_{test}^{(m)}$ , which result from partitioning  $S^{(m)}$ . However, unlike classification, the procedure for generating these consists of the following steps:

- *Step 1* -  $S_{train}^{(m)}$  is obtained from the set  $S_{train} \triangleq \{(\mathbf{x}_i, m_i), i = 1, 2, \dots, N_{train}^{(z)}\}$  (in one-to-one correspondence with  $S_{train}^{(z)}$ ) by discarding all the data associated with a value of their index  $i$  such that  $z_i = -1$  (in other words, the data associated with those locations at which the transmitted signal is not correctly received are ignored).
- *Step 2* - Similarly as  $S_{train}^{(m)}$ ,  $S_{test}^{(m)}$  is obtained from the set  $S_{test} \triangleq \{(\mathbf{x}_i, y_i), i = N_{train}^{(z)} + 1, \dots, N_{train}^{(z)} + N_{test}^{(z)}\}$  (in one-to-one correspondence with  $S_{test}^{(z)}$ ) by discarding all the data associated with a value of their index  $i$  such that  $z_i = -1$ .

An additional procedure for further reducing the amount of data included in  $S_{train}^{(m)}$  is carried out within step 2 when our classification and regression models are trained on the basis of a set of measurements that have not been acquired in the same environment as that for which the identification of the coverage area and the prediction are accomplished; this procedure involves the function  $d(\mathbf{x})$  (16) and is described in Paragraph IV-C. Generally speaking, our set generation method results in a training set  $S_{train}^{(m)} \triangleq \{(\tilde{\mathbf{x}}_i, \tilde{m}_i), i = 1, 2, \dots, N_{train}^{(m)}\}$  and in a test set  $S_{test}^{(m)} \triangleq \{(\tilde{\mathbf{x}}_i, \tilde{m}_i), i = N_{train}^{(m)} + 1, N_{train}^{(m)} + 2, \dots, N_{train}^{(m)} + N_{test}^{(m)}\}$ ; here, the notation  $(\tilde{\mathbf{x}}_i, \tilde{m}_i)$  has been adopted in place of  $(\mathbf{x}_i, m_i)$  since a renumbering of the remaining data is done at the end of step 2 within each set; moreover  $N_{train}^{(m)}$  and  $N_{test}^{(m)}$  denote the number of elements of  $S_{train}^{(m)}$  and  $S_{test}^{(m)}$ , respectively. Then,  $S_{train}^{(m)}$  is processed by a  $\epsilon$  - *support vector regression* ( $\epsilon$ -SVR) algorithm [23]. This requires solving the (primal) optimization problem

$$\min_{\tilde{\mathbf{w}}, \tilde{b}, \tilde{\xi}, \tilde{\xi}^*, \epsilon} \frac{1}{2} \tilde{\mathbf{w}}^T \tilde{\mathbf{w}} + \tilde{C} \sum_{i=1}^{N_{train}^{(y)}} \tilde{\xi}_i + \tilde{C} \sum_{i=1}^{N_{train}^{(y)}} \tilde{\xi}_i^* \quad (17)$$

subject to

$$\tilde{\xi}_i, \tilde{\xi}_i^* \geq 0, \quad (18)$$

$$\mathbf{w}^T \phi(\tilde{\mathbf{x}}_i) + \tilde{b} - \tilde{m}_i \leq \epsilon + \tilde{\xi}_i \quad (19)$$

and

$$\tilde{m}_i - \mathbf{w}^T \phi(\tilde{\mathbf{x}}_i) - \tilde{b} \leq \epsilon + \tilde{\xi}_i^*, \quad (20)$$

with  $i = 1, 2, \dots, N_{train}^{(m)}$ . The meaning of most parameters and vectors appearing in the new problem is similar to that

illustrated for the related problem (9)-(11); note, in particular, that  $\tilde{\xi}_i^*$ , with  $i = 1, 2, \dots, N_{train}^{(m)}$ , is a slack variable appearing in the new constraint (20),  $\tilde{\xi} \triangleq [\tilde{\xi}_1, \tilde{\xi}_2, \dots, \tilde{\xi}_l]^T$  and that  $\tilde{C} > 0$  is a regularization parameter modifying the weight of the errors appearing in the regression procedure. However, in this case, the constraints (19) and (20) contain the additional real parameter  $\epsilon > 0$ , which represents the width of the called  $\epsilon$ -insensitive tube (i.e., a measure of the precision of regression). In our work  $\epsilon = 3$  has been selected on the basis of: a) the measurement noise intensity (see (7)) estimated in our measurement campaign; b) a trial and error procedure adopted to assess the sensitivity of the  $\epsilon$ -SVR procedure to the parameter  $\epsilon$ . Once the value of  $\epsilon$  is selected, similarly as the classification technique, the only parameters whose values need to be properly adjusted in the  $\epsilon$ -SVR technique are  $\tilde{C}$  and  $\tilde{\gamma}$  (the last one is contained in the kernel function).

Reformulating the optimization problem (17)-(20) as a Lagrangian problem leads easily to the *dual problem*

$$\begin{aligned} \min_{\tilde{\alpha}, \tilde{\alpha}^*} \quad & \frac{1}{2} (\tilde{\alpha} - \tilde{\alpha}^*)^T \tilde{\mathbf{Q}} (\tilde{\alpha} - \tilde{\alpha}^*) + \epsilon \sum_{i=1}^{N_{train}^{(y)}} (\tilde{\alpha}_i + \tilde{\alpha}_i^*) \\ & + \sum_{i=1}^{N_{train}^{(y)}} \tilde{m}_i (\tilde{\alpha}_i - \tilde{\alpha}_i^*) \end{aligned} \quad (21)$$

subject to

$$\tilde{\mathbf{e}}^T (\tilde{\alpha} - \tilde{\alpha}^*) = 0 \quad (22)$$

and

$$0 \leq \tilde{\alpha}_i, \tilde{\alpha}_i^* \leq \tilde{C}, \quad (23)$$

with  $i = 1, 2, \dots, N_{train}^{(m)}$ . Here,  $\tilde{\mathbf{e}} = [1, 1, \dots, 1]^T$  is the  $N_{train}^{(m)}$ -dimensional vector of all ones,  $\tilde{\alpha} = [\tilde{\alpha}_1, \tilde{\alpha}_2, \dots, \tilde{\alpha}_{N_{train}^{(m)}}]^T$  and  $\tilde{\alpha}^* = [\tilde{\alpha}_1^*, \tilde{\alpha}_2^*, \dots, \tilde{\alpha}_{N_{train}^{(m)}}^*]^T$  are  $N_{train}^{(m)}$ -dimensional vectors collecting the (positive) Lagrange multipliers, and  $\tilde{\mathbf{Q}} = [\tilde{Q}_{i,j}]$  is a  $N_{train}^{(m)} \times N_{train}^{(m)}$  positive semidefinite matrix, with  $\tilde{Q}_{i,j} = K(\tilde{\mathbf{x}}_i, \tilde{\mathbf{x}}_j)$  (note that in our approach the mapping  $\phi(\mathbf{x})$  and the kernel function  $K(\mathbf{x}, \hat{\mathbf{x}})$  are the same as those employed in the classification algorithm described above). Solving the problem (21)-(23) produces the solutions  $\tilde{\alpha}_o = [\tilde{\alpha}_{o,1}, \tilde{\alpha}_{o,2}, \dots, \tilde{\alpha}_{o,N_{train}^{(m)}}]^T$  and  $\tilde{\alpha}_o^* = [\tilde{\alpha}_{o,1}^*, \tilde{\alpha}_{o,2}^*, \dots, \tilde{\alpha}_{o,N_{train}^{(m)}}^*]^T$  for the vectors  $\tilde{\alpha}$  and  $\tilde{\alpha}^*$ , respectively, and  $\tilde{b}_o$  for  $\tilde{b}$ ; this allow us to evaluate the *predictive function*

$$p(\mathbf{x}) \triangleq \sum_{i=1}^{N_{train}^{(m)}} (\tilde{\alpha}_i^* - \tilde{\alpha}_i) K(\tilde{\mathbf{x}}_i, \mathbf{x}) + \tilde{b}_o, \quad (24)$$

which represents the solution to our regression problem.

Finally, it is worth pointing out that:

- The accuracy of the field strength prediction provided by the predictive function  $p(\mathbf{x})$  (24) is influenced not only by the data contained in the training set  $S_{train}^{(m)}$ , but also by our specific choice for the values of the parameters  $\tilde{C}$  and  $\tilde{\gamma}$ . The optimization of these parameters is accomplished on the basis of the test set  $S_{test}^{(m)}$  and of a specific performance measure, and involves a cross-validation procedure; this is discussed in more detail in Paragraph V-A.

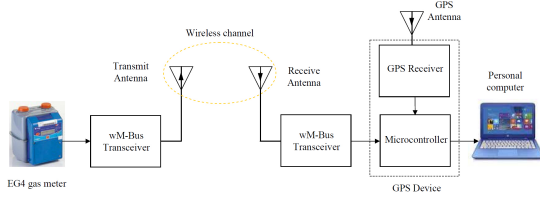


Fig. 1: Block diagram of the hardware tools employed in our measurement campaign.

- Our approach exploits both a classification technique for delimiting the coverage area and a regression technique for estimating the field strength inside it. In previous work investigating the application of SVM to field strength prediction (see [10], [16] and [18]), the use of SVM-based regression only has been proposed, so that the system coverage area is generated as a by-product of the adopted regression method. However, our numerical results have evidenced that the last approach may result in an appreciably less accurate estimate of the coverage area with respect to the method we propose in this manuscript.

### III. MEASUREMENT TOOLS AND CAMPAIGNS

In this Section a short description of the measurement tools and of the hardware set-up adopted in our measurement campaigns is provided. Then, some relevant information about the scenarios considered in such campaigns and various specific guidelines followed in acquiring our measurements are illustrated.

#### A. Measurement tools and set-up

As already mentioned in Paragraph II-A, we are interested in measuring the outdoor propagation losses in a wireless star network consisting of a data concentrator serving multiple gas meters. A block diagram of the hardware tools employed in our measurement campaigns is shown in Fig. 1. In practice, to ease data acquisition, a commercial gas meter, equipped with a 169 MHz transceiver and placed in a *fixed* outdoor location (of potential interest for the installation of a data concentrator), has been used for accomplishing wireless data transmission; on the other hand, a data acquisition hardware, including another 169 MHz transceiver, a GPS receiver and a portable PC, has been placed on a car moving at a limited and approximated constant speed in a wide area surrounding the transmitter. Some relevant technical information about the transmitter, the data acquisition device and its output information are provided below.

- 1) *Transmitter*- This device is made of a EG4 gas meter [24] manufactured by the Italian company Meter Italia (which is a subsidiary company of CPL Concordia) and a wireless M-Bus transceiver, operating according to the mode N1c of EN 13757-4:2013 [2] and transmitting<sup>6</sup> a new meter reading every 3 s. In practice, a new data

<sup>6</sup>Unluckily, technical information about the transmit antenna employed in this gas meter cannot be made public.

packet, consisting of 46 bytes (35 of which form the payload), is radiated every 3 s; each packet contains the gas meter address and a fictitious gas reading (since the gas meter is not connected to a gas network), and its transmission lasts about 0.153s (since the bit rate for 2a channel of the N1c mode is equal to 2.4 kbps); one of the following power levels can be selected for data transmission: 21 dBm, 24 dBm, 27 dBm and 30 dBm.

- 2) *Data acquisition hardware* - This device has been explicitly designed and implemented for our measurement campaigns (see Fig. 2). It consists of: a) a receiver board based on a wireless M-Bus transceiver RC1701HP-MBUS, manufactured by Radiocrafts [25] and characterized by a nominal sensitivity<sup>7</sup> equal to -119 dBm; b) a Sirio SKB antenna [26] (i.e., a  $\lambda/4$  omnidirectional antenna for the VHF band) feeding the transceiver and installed on the roof of a car (the roof behaves like a ground plane; see Fig. 3); c) an AM50 GPS receiver manufactured by GeoShack [27] and equipped with an external antenna; d) a portable computer. The data acquisition hardware operates as follows. A new estimate of the strength of the signal received from the gas meter of interest, together with the meter address, is sent to a microcontroller embedded in the GPS module every 3 s; these information are tagged by an estimate of the car position provided by the GPS receiver and then sent to a portable computer (through a serial port), where they are displayed in real time and stored in a text file.
- 3) *Available information* - The data available on the personal computer include the following information: date, timing, longitude and latitude (expressed in decimal degrees), altitude (expressed in m), car speed (expressed in m/s), car direction, number of GPS satellites, meter address and an RSS *indication* (RSSI, expressed in dBm) averaged over the considered data packet.

#### B. Measurement campaigns: selected scenarios and guidelines followed in data acquisition

Our measurement campaigns have mainly concerned densely populated areas of cities and villages in northern Italy (i.e., *urban* and *suburban* scenarios), because of their relevance in the deployment of new infrastructures for gas metering. The considered areas have partitioned into two classes, the first one (class #1) including the villages and the cities located in the Po valley<sup>8</sup> (i.e., characterized by a *flat* terrain), the second one (class #2) encompassing villages located on the Italian Alps or on the Tuscan-Emilian Apennine (i.e., characterized by a *hilly* or *mountainous* terrain); further details about the selected areas are given in Section V. As it will become clearer in Section IV-A, our classification of the selected geographical areas is based on the fact that, when the points at which measurements

<sup>7</sup>Our transceiver is unable to detect the transmitted signal if its strength is below this threshold. For this reason, as already mentioned above, a power level of  $P_{NC} = -120$  dBm has been conventionally selected to denote the lack of radio coverage at a specific location.

<sup>8</sup>This is a large and flat area delimited by the Italian Alps, the Adriatic sea and the Tuscan-Emilian Apennine.



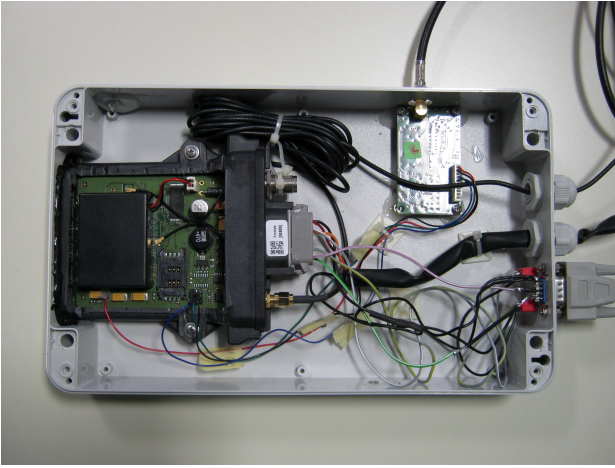


Fig. 2: Data acquisition device employed in our measurement campaigns (the antenna and the portable computer connected to this device are not visible in this photograph).

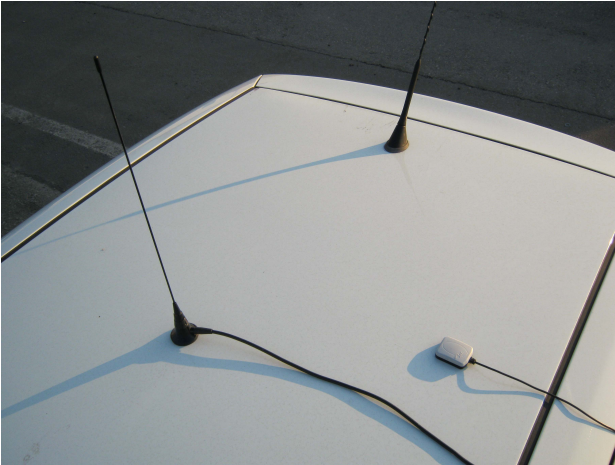


Fig. 3: Sirio SKB antenna (on the left) and GPS antenna (on the right) employed by our data acquisition hardware installed on the roof of the car employed in our measurement campaign.

are collected in a given area are characterized by significantly different altitudes, a couple of specific features, which are not taken into consideration for flat terrains, are employed in SVM classification and regression; vice versa, feature extraction for flat terrains entails the evaluation of two features which are ignored in the other case.

In our work the following two specific tasks have been carried out before starting a new measurement campaign in each of the selected urban scenarios:

- 1) *Partitioning of the considered scenario into districts* - Large urban areas have been usually partitioned into districts characterised by similar propagation conditions. This step is motivated by our interest in comparing field strength models referring to different cities or villages, but whose data have been collected in districts exhibiting a significant degree of similarity in terms of street widths, building densities, building heights, building age and vegetation.

- 2) *Selection of transmitter locations* - In each district favorite locations for our transmitter have been identified by looking for proper positions of data concentrators. Note that, first of all, such positions should be easily accessible to ease the installation of the transmitter; moreover, when possible, they should be sufficiently high to ensure a large coverage area within the considered district. Unluckily, we were often unable to access relevant sites characterized by a significant height, so that the height of the transmitter usually ranged from 1,5 m to 1,8 m (a few high positions, available on different buildings, were available in the city of Modena and in the village of Rocca Malatina only). However, it should be expected that, in any future infrastructure for gas metering, heterogeneous sites, characterized by significantly different heights, will be available.

After this preliminary work, the transmitter has been installed in one of the selected locations and RSS data have been acquired in all the roads of the considered district and its neighborhoods travelling at an almost constant speed (25 km/h); this has allowed us to achieve a uniform spatial sampling of the considered area and to maximise the diversity of the acquired data. As far as the last point is concerned, it is important to mention that, in each measurement campaign, we have tried to collect similar quantities of measurements for the coverage area and for the area outside it, since, as evidenced by our computer simulations, this improves the accuracy of our classification method. Note that, generally speaking, the availability of balanced quantities of data associated with the presence of radio coverage and with the lack of it helps a classification algorithm to learn to discriminate between these two different conditions. At the same time, a sufficiently large number of points acquired in the coverage area improves the prediction capability of the employed regression algorithm.

#### IV. DATA PROCESSING AND SOFTWARE TOOLS

As explained in the previous Section, each measurement campaign has resulted in a set of RSS measurements referring to a specific district of a given town or village; each measurement is tagged by the GPS coordinates of the location at which it has been acquired. In this Section we provide some additional details about the processing techniques employed to predict a coverage area and a RSS map on the basis of the available measurements. In particular, we first describe the procedure we adopted to extract a set of features from each of the considered locations. Then, we take into consideration SVM processing again, and discuss some specific choices we made in implementing it. Finally, we comment on our software implementation of the proposed method and briefly illustrate the potentialities of the SVM-based software tool we developed for radio planning in the 169 MHz band.

##### A. Extraction of significant features

In this Section we assume that, for a given location of the transmitter,  $N$  measurements have been collected at  $N$  distinct and known locations in its neighborhoods. Before starting SVM classification, three groups of geometric features are

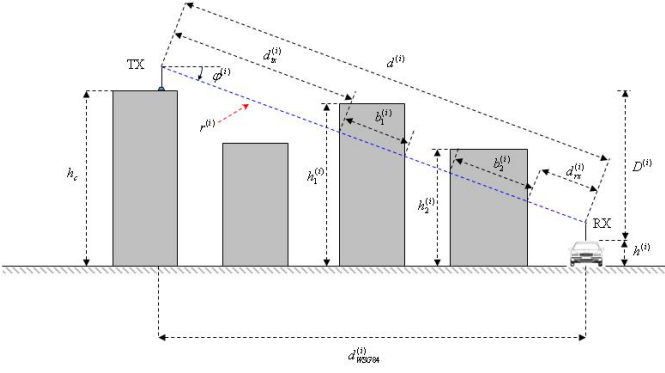


Fig. 4: Schematic representation of an urban scenario in which the line-of-sight wireless link between a transmitter and a receiver is blocked by multiple buildings.

evaluated for the  $i$ -th location (with  $i = 1, 2, \dots, N$ ) on the basis of: a) the positions of the transmitter and the receiver, b) a 3D geometrical representation of the considered propagation environment (in practice, a digital map). The first group, which is computed on the basis of the positions of the transmitter and the receiver only, consists of the following three features (see Fig. 4):

- 1) *Transmitter-receiver differential height* - This feature is defined as

$$D^{(i)} \triangleq h_c - h^{(i)}, \quad (25)$$

where  $h_c$  denotes the altitude of the *transmitter* (TX) and  $h^{(i)}$  the altitude of the  $i$ -th position for the *receiver* (RX) (each altitude is measured with respect to the support of the corresponding antenna).

- 2) *Transmitter-receiver distance* - The distance between the transmitter and the  $i$ -th position is evaluated as

$$d^{(i)} = \sqrt{(D^{(i)})^2 + (d_{WGS84}^{(i)})^2}, \quad (26)$$

where  $D^{(i)}$  is given by (25) and  $d_{WGS84}^{(i)}$  represents the distance between the considered positions evaluated on the basis of their WGS-84 coordinates<sup>9</sup>. Note that  $d^{(i)}$  represents the length of the segment  $r^{(i)}$  connecting the transmitter to the receiver, as illustrated in Fig. 4.

- 3) *Angular deviation* - This feature (denoted  $\varphi^{(i)}$  in Fig. 4) represents the elevation angle of the RX antenna measured with respect to the TX antenna; note that in our measurements the employed antennas exhibit an omnidirectional pattern on their azimuth planes and that they are never tilted. The adoption of this feature is motivated by the fact that such antennas do not have an omnidirectional pattern on the elevation plane, so that an angular deviation different from zero may have a significant impact on propagation losses.

The second group of features depends not only on the positions of the transmitter and the receiver, but also on the positions and geometry of the buildings preventing *line of sight* (LOS)

<sup>9</sup>In practice, the Vincenty's inverse method [28] is used to compute the geographical distance  $d_{WGS84}^{(i)}$  between the TX and RX locations on the basis of their GPS coordinates.

propagation, as illustrated in Fig. 4; in particular, these features aim at capturing some relevant properties of key obstructions. In the following, it is assumed that at the  $i$ -th position of the receiver (with  $i = 1, 2, \dots, N$ ) the view of the transmitter is obstructed by  $K^{(i)}$  buildings, whose heights are denoted  $\{h_l^{(i)}, l = 1, 2, \dots, K^{(i)}\}$  (note that  $K^{(i)} = 2$  in Fig. 4). Moreover, the length of the portion of the segment  $r^{(i)}$  intersecting the  $l$ -th building is denoted  $b_l^{(i)}$ . Given these definitions, the following five features are evaluated at the  $i$ -th location:

- 1) *Maximum height of blocking buildings* - This feature is defined as

$$h_{max}^{(i)} \triangleq \max_l h_l^{(i)} \quad (27)$$

and provides information about the maximum degree of the vertical obstruction along the  $r^{(i)}$  direction.

- 2) *Average height of blocking buildings* - This feature is defined as

$$h_{av}^{(i)} \triangleq \frac{\sum_{l=1}^{K^{(i)}} h_l^{(i)}}{K^{(i)}} \quad (28)$$

and provides information about the average degree of the vertical obstruction encountered along the  $r^{(i)}$  direction.

- 3) *Portion through buildings (PTB)* - This feature is evaluated on the basis of the formula

$$PTB^{(i)} \triangleq \frac{\sum_{l=1}^{K^{(i)}} b_l^{(i)}}{d^{(i)}} \quad (29)$$

and provides information about the portion of  $r^{(i)}$  included in the blocking buildings.

- 4) *Distance between transmitter and its closest building* - This feature, denoted  $d_{tx}^{(i)}$  in Fig. 4, represents the distance between the transmitter and its closest building, measured along the  $r^{(i)}$  direction. Its use is motivated by the fact that the building closest to the transmitter is expected to have a significant influence on the attenuation of the transmitted signal.

- 5) *Distance between receiver and its closest building* - This feature, denoted  $d_{rx}^{(i)}$  in Fig. 4, represents the distance between the receiver and its closest building, measured along the  $r^{(i)}$  direction. This feature is the dual of the previous one.

The last group consists of a single feature, namely the so-called *portion through ground* (PTG), which plays a fundamental role in the presence of an uneven terrain. The definition of this quantity is very similar to that of  $PTB^{(i)}$  (29), since it refers to the case in which the view of the transmitter is obstructed by ground at the receive side; in this case we assume that, generally speaking, the segment  $r^{(i)}$  connecting the transmitter to the receiver intersects ground  $N^{(i)}$  times and that  $a_l^{(i)}$  denotes the length of its  $l$ -th intersection (with  $l = 1, 2, \dots, N^{(i)}$ ). Then, the PTG at the  $i$ -th location is defined as

$$PTG^{(i)} \triangleq \frac{\sum_{l=1}^{N^{(i)}} a_l^{(i)}}{d^{(i)}}, \quad (30)$$

with  $i = 1, 2, \dots, N$ .

Independently of the class the analysed area belongs to, in our data processing procedure the following five features have



been computed: transmitter-receiver distance, angular deviation, maximum height of blocking buildings, average height of blocking buildings and PTB. Moreover, the following two features have been computed for class #1 only: distance between transmitter and its closest building, and distance between receiver and its closest building. On the contrary, the remaining two features (namely, transmitter-receiver differential height and PTG) have been computed for class #2 only. Therefore, whatever the class of the analysed area, the feature extraction procedure generates a set  $S^{(\tilde{x})} \triangleq \{\tilde{\mathbf{x}}_l, l = 1, 2, \dots, N\}$  of seven dimensional vectors (here,  $\tilde{\mathbf{x}}_l = [\tilde{x}_l^{(1)}, \tilde{x}_l^{(2)}, \dots, \tilde{x}_l^{(m)}]^T$  with  $m = 7$ ), which, as discussed in the following Paragraph, are pre-processed before feeding the classification and regression algorithms illustrated in Section II-B.

Finally, it is worth mentioning that:

- 1) All the features defined above have a geometric meaning. However, it is well known that, generally speaking, radio propagation in a given environment is influenced by a number of factors among which an important role may be played by atmospheric conditions. Fluctuations of a few dBm were observed in the received power when the transmitter and the receiver were held at fixed locations for some days; however, we were unable to separate the contribution originating from atmospheric factors (e.g., humidity and temperature) from those due to other environmental changes occurring in the neighborhoods (e.g., reflection and blocking due to vehicles, pedestrians and other objects on close roads).
- 2) The selection of the features employed in our work has been inspired, in part, by previous work and, in particular, by [16]. Moreover, extensive computer simulations have been run to experimentally assess the relevance of each feature, i.e. its impact on the accuracy of the considered SVM-based methods. Our numerical results have evidenced that a good accuracy can be achieved if the sets of features defined above are adopted. Note that these sets are small so that *dimensionality reduction techniques* [9] are not needed. On the contrary, a larger number of features is evaluated in [16], since the segment  $r^{(i)}$  connecting the transmitter to the receiver (see Fig. 4) is partitioned into multiple intervals, and three distinct features are evaluated for each interval; for this reasons, *principal component analysis* and *nonlinear principal component analysis* are used in that case to reduce the dimensionality of the feature space before SVM-based processing in order to prevent the well known *overfitting* phenomenon.

### B. Data Pre-Processing and SVM Processing

The extraction of the features defined in the previous Paragraph is followed by data pre-processing (in particular, data scaling) and SVM processing (whose mathematical details have been illustrated in Section II-B). In the following we describe the method we adopted for data scaling and then provide some additional details about the SVM processing we implemented.

- *Data scaling* - Data scaling is usually employed in SVM applications when the components of feature vectors are characterized by substantially different ranges and, in particular, some of them may take on large values. In fact, when this occurs, large components may hide the contribution of the remaining ones in the evaluation of kernel values<sup>10</sup>; this unavoidably entails various numerical problems, resulting in a loss of accuracy. In the considered problem the ranges of some components of the feature vector  $\tilde{\mathbf{x}}_l = [\tilde{x}_l^{(1)}, \tilde{x}_l^{(2)}, \dots, \tilde{x}_l^{(m)}]^T$  (with  $m = 7$  and  $l = 1, 2, \dots, N$ ) are substantially different (see (25)-(30)), so that scaling is indispensable. For this reason, in our work the vector  $\tilde{\mathbf{x}}_l$  is mapped into the scaled feature vector  $\mathbf{x}_l = [x_l^{(1)}, x_l^{(2)}, \dots, x_l^{(m)}]^T$  for any  $l$ ; the adopted mapping rule can be expressed as

$$x_l^{(i)} = \frac{\tilde{x}_l^{(i)} - \mu_i}{\delta_i} \quad (31)$$

with  $i = 1, 2, \dots, m$ , where  $\mu_i$  and  $\delta_i$  denote the mean value and the standard deviation, respectively, of the  $i$ -th feature. This leads to generating the new set of feature vectors  $S^{(x)} \triangleq \{\mathbf{x}_l, l = 1, 2, \dots, N\}$ , which feeds our SVM-based classification and regression techniques.

- *Selection of the kernel function* - In the SVM literature various options are available for the kernel function; in particular, the most common options are the linear, polynomial, sigmoid and *radial basis function* (RBF) kernels (e.g., see [21, Sec. 1] and [22, Par. 4.3]). Generally speaking, the RBF kernel

$$K(\mathbf{x}, \mathbf{y}) = \exp(-\gamma \|\mathbf{x} - \mathbf{y}\|^2), \quad (32)$$

is the most reasonable choice in a number of problems (here,  $\gamma$  is a real positive parameter). In fact, this kernel has a number of good features, since it can properly handle the cases in which the relation between class labels and features is nonlinear in classification problems, it depends on a single hyper-parameter ( $\gamma$ ) and its use does not usually entail numerical problems [21, Sec. 3], [9].

- *Performance metrics* - In our technique the training phases of SVM-based classification and SVM-based regression are followed by a validation phase in which the accuracy of the trained models for classification and for signal strength prediction, respectively, is assessed. In our work the evaluation of *classification accuracy* is based on the following performance metrics: a) accuracy; b) full-scale accuracy; c) percentage of false positives. The *accuracy* (denoted  $A$  in the following) is defined as

$$A = \frac{N_{cc}}{N_t^{(z)}} \cdot 100\%, \quad (33)$$

where  $N_t^{(z)}$  is the overall number of elements of the test set  $S_{test}^{(z)}$  selected in the classification procedure and  $N_{cc}$  is the number of points belonging to the same set and correctly classified (in other words,  $N_{cc}$  represents the overall number of true positives and true negatives). A

<sup>10</sup>Note that typical kernels depend on feature vectors through their inner products.

similar definition is adopted for the *full-scale accuracy*  $A_{fs}$ , which, however, does not refer to the entire  $S_{test}^{(z)}$ , but only the portion of its points characterized by a RSS belonging to the interval [-119 dBm, -110 dBm] or equal to -120 dBm; note that this parameter has a significant practical relevance, since it refers to the cases in which RSS is close to receiver sensitivity (this usually occurs, for instance, at receiver positions close to the borders of the considered coverage area). The *percentage of false positives* (denoted  $P_{fp}$  in the following) is defined as the percentage of points of the test set  $S_{test}^{(z)}$  which are erroneously assigned to the coverage area by the classification algorithm.

On the other hand, the evaluation of *regression accuracy* is based on the evaluation of the *root mean square error* (RMSE), which is defined as

$$RMSE \triangleq \sqrt{\frac{\sum_{i=N_{train}^{(m)}+1}^{N_{train}^{(m)}+N_{test}^{(m)}} (\hat{m}_i - \tilde{m}_i)^2}{N_{test}^{(m)}}}, \quad (34)$$

where  $\hat{m}_i$  is the RSS value predicted at the same location as the measurement  $\tilde{m}_i \in S_{train}^{(m)}$  and  $N_{test}^{(m)}$  is the overall number of elements of the test data set for SVM regression.

### C. Implementation of the Proposed SVM-Based Method for Radio Planning

A complete software tool based on the proposed method for SVM-based radio planning has been implemented in MATLAB; this allowed us to benefit from the availability of various existing packages for this environment and to easily develop a user friendly *graphical user interface* (GUI). In the development of this tool the following two specific problems had to be solved:

- 1) the automatic extraction of the feature vectors for all the locations at which RSSI data were acquired during each measurement campaign;
- 2) the implementation of SVM methods.

The first problem has been solved as follows. As already mentioned above, 3D maps of the considered environments have been downloaded from public regional databases collecting topographic information or made available by Italian regional offices for research purposes; in all the considered cases the available maps were in *shapefile* (.shp) format. After acquiring the map of the environment of interest, a preliminary check has been accomplished to assess the quality of its content (i.e., of the geographical data it contained) and verify that its format<sup>11</sup> was ready to be correctly interpreted by our software tool. This task has been carried out by means of the open source software QGIS [29]; in fact, this has allowed us to easily access the map *layers* referring to: a) 3D representations of buildings; b) contour lines for the considered area; c) roads. Note

that, on the one hand, building heights and the geographical coordinates of building corners are needed to evaluate the features  $h_{max}^{(i)}$  (27),  $h_{av}^{(i)}$  (28),  $PTB^{(i)}$  (29),  $d_{tx}^{(i)}$  and  $d_{tx}^{(i)}$  (see Fig. 4). On the other hand, the knowledge of contour lines is certainly required in the evaluation of  $PTG^{(i)}$  (30) for any area belonging to class # 2; however, in a hilly/mountainous environment these information also play a fundamental role in the evaluation of the differential altitude  $D^{(i)}$  (25), the distance  $d^{(i)}$  (26) and the angular deviation  $\varphi^{(i)}$  (see Fig. 4). In fact, level curves can be employed to evaluate the altitude of an arbitrary point by means of a simple interpolation function, since adjacent curves are usually characterized by a constant spacing. In principle, as already mentioned in Paragraph II-A, map information about the roads crossing the considered area are not required. In practice, however, they have been useful in densely populated areas characterized by high buildings. In fact, in those cases the acquired GPS positions were often affected by non negligible errors because of poor reception conditions; when this occurred, errors have been mitigated projecting each estimated position onto the central line of the road in which GPS signals have been acquired.

After properly checking the format and content of the map of the considered area, map information have been processed to compute the feature vectors for all the locations at which measurements were acquired. Note that the implementation of this task has been substantially simplified by the use of the Mapping Toolbox [30], which has allowed us to import the needed geographical data in the Matlab environment.

The second problem, i.e. the implementation of SVM methods, has been easily solved thanks to the availability of a public library for SVM methods, called LIBSVM [31].

In developing our software implementation of the adopted SVM-based methods (our implementation is called *SVM-based Tool for Radio Planning*, SVMTRP, in the following) three different *prediction modes* (PMs) were taken into consideration in order to satisfy all the needs envisaged for the future radio planning of gas metering networks. A short description of the aim, input data, data processing tasks and resulting outputs is provided below for each of these PMs.

**PM #1 - Aim:** this mode allows to assess the accuracy of the classification and regression techniques implemented in our study; it should be considered as a tool for assessing the prediction capability of the employed methods.

**Input data:** geographical data of the measurement area, TX coordinates and height, RX height, set of measurements (each tagged by the GPS coordinates of the location at which it has been acquired).

**Data processing:** the accomplished tasks have been described in detail in Paragraph II-B; consequently, no additional detail is provided here.

**Outputs:** RMSE and accuracy evaluated over the test set of SVM regression and classification, respectively.

**PM #2 - Aim:** for a given position of one or more data concentrators and in the absence of measurements acquired for the considered environment, this mode provides the following information for each concentrator: a) a prediction of its coverage area; b) a prediction of the RSS at the nodes of rectangular lattice overlapping the considered environment.

<sup>11</sup>Note that our preliminary analysis of the available maps represents an unavoidable task, because of the lack of a national standard for open geographical data in Italy; for this reason different Italian regions may not follow the same guidelines in this field.

In this case, such predictions are based on classification and regression models generated for environments *different* from the considered one (and for which measurement campaigns have been accomplished): for this reason they are called “blind predictions” in the following<sup>12</sup>. It should be expected that the predictions generated in this case are realistic if the adopted classification and regression models have been originally computed for an environment having a structural resemblance (in terms of building density and typology, vegetation, street widths, etc.) with that for which the blind predictions are evaluated. In practice, this PM can be very useful in radio planning when assessing the suitability of various options for the positioning of concentrators in a given area.

*Input data:* geographical data of the considered area, coordinates and height of the selected data concentrators (transmitters), RX height, lattice parameters (coordinates of two opposite corners and lattice step sizes).

*Data processing:* for each available concentrator all the features are evaluated at the locations corresponding to vertices of the selected rectangular lattice; then, regression and classification models trained for environments different from the considered one are used for prediction over the considered area.

*Outputs:* for each concentrator a RSS prediction over the vertices of the selected lattice and a prediction of the coverage area are produced (in particular, RSS prediction results are represented as a colour map); moreover, a colour map showing, for each point of the considered area, the best concentrator serving it (i.e., the one from which the strongest signal is received) is generated (such a map is called *best server map* and is characterized by as many distinct colours as the overall number of concentrators, as illustrated in the following Section).

**PM #3 - Aim:** for a given position of a concentrator, this mode allows to assess the generalization capability of a given trained model. In fact, similarly as PM #2, it generates a RSS blind prediction, being based on a regression model resulting from data acquired in environments *different* from (but, hopefully, structurally similar to) the considered one. However, unlike PM #2, measurements are actually available for the considered environment, so that the accuracy of blind predictions can be assessed at the locations at which such measurements have been acquired. It is important to point out that, in this PM, the set of elements forming  $S_{test}^{(m)}$  (and consisting of real measurements for the considered area) is further reduced within the step 2 of the procedure adopted for generating it (see Paragraph II-B); in fact, any datum  $\mathbf{x}_i \in S_{test}$  such that  $d(\mathbf{x}_i) = -1$  (see (16)) is discarded. This choice is motivated on the fact that, in this case, a fair assessment of the prediction accuracy is obtained if only the data that, on the basis of our classification algorithm, refer to the locations belonging to the estimated coverage area are taken into consideration.

*Input data:* geographical data of the measurement area, TX coordinates and height, RX height, set of measurements (each

tagged by the GPS coordinates of the location in which it has been acquired).

*Data processing:* for the considered concentrator all the features are evaluated at the positions associated with the considered measurements; then, regression and classification models trained for environments different from the considered one are used for RSS prediction over the considered area.

*Outputs:* coverage area prediction and RSS prediction for the positions at which the available measurements have been acquired; RMSE, accuracy, full scale accuracy and percentage of false positives evaluated on the basis of the available measurements.

## V. NUMERICAL RESULTS

In this Section various numerical results generated by our radio planning tool (called SVMTRP) on the basis of the data sets collected in our measurement campaigns are illustrated. In such campaigns the following relevant choices have been made:

- 1) The lowest output power level (21 dBm) has been selected for the transmitter employed in our measurement set-up (see Fig. 1); for this reason, the resulting coverage area represents the worst case associated with a given position of the transmitter.
- 2) The measurements for the first class of propagation environments (i.e., for class #1) have been acquired in various districts of the cities of Modena, Bologna and Ferrara, and in relevant areas of the villages of Carpi and Concordia sulla Secchia (both belonging to the Modena province). The overall number of measurements collected for class #1 is equal to 16009.
- 3) The measurements for the second class of propagation environments (i.e., for class #2) have been acquired in various relevant areas of the villages of Guiglia, Zocca and Rocca Malatina (all belonging to the Modena province) and Isera (belonging to the Trento province). Note that, on the one hand, Guiglia, Zocca and Rocca Malatina are located in the same upland of the Tuscan-Emilian Apennine, whereas, on the other hand, Isera is located on the side of a mountain in the Trentino - Alto Adige region. For this reason, the considered cases cover the typical land conformation of villages in mountainous/hilly areas of northern Italy. The overall number of measurements collected for class #2 is equal to 11391.
- 4) In any propagation environment, when possible, at least one thousand measurements have been acquired.
- 5) In the considered cases the 3D maps needed by SVMTRP have been acquired from the topographic database of the Emilia-Romagna region [32] or from that of the autonomous province of Trento [33]. All these maps are available in shapefile format.

### A. Parameters optimization

As already mentioned in Section II-B, both classification and regression require the optimization of a couple parameters,

<sup>12</sup>The concept of *bootstrapping a propagation model* with measurements acquired in a given environment and then using it in other environments is not new in the technical literature (e.g., see [5, Par. IV-B] and references therein).

namely  $(C, \gamma)$  and  $(\tilde{C}, \tilde{\gamma})$ , respectively. In our work two different strategies have been adopted to solve this optimization problem, one for PM #1, the second for one for PMs #2 and #3. This choice is due to the fact that, in the case of PM #1, we are interested in adjusting the values of the couples  $(C, \gamma)$  and  $(\tilde{C}, \tilde{\gamma})$  in way that the *classification and regression accuracies are maximised over test sets*. On the contrary, in the case of PMs #2 and #3, our selection of these parameters should optimize the *generalization capability* of our SVM-based methods so that in a given environment reliable prediction can be evaluated on the basis of a set of measurements acquired in *different* areas. In practice, in the first case, the *grid-search* method illustrated in [21] has been adopted. This is based on an exhaustive search over a finite set of values for the couple  $(C, \gamma)$  (or, equivalently,  $(\tilde{C}, \tilde{\gamma})$ ), so that the best option, in terms of accuracy ( $A$ ) for classification and RMSE for regression can be found over the available test sets. In the other case, a grid-search method has been also used, but in a different way. In fact, first of all, a lower bound on the accuracy (denoted  $A_{lb}$ ) and an upper bound on the RMSE (denoted  $RMSE_{ub}$ ) have been fixed. Then, in the optimisation of the classification (regression) technique we have searched for, over the given grid, all the values of the couple  $(C, \gamma)$  ( $(\tilde{C}, \tilde{\gamma})$ ) ensuring an accuracy (RMSE) greater than  $A_{lb}$  (lower than  $RMSE_{ub}$ ). Finally, among the selected couples, the one characterized by the smallest value of  $\gamma$  has been chosen. Note that in this procedure it may occur that, in the set of possible values for the couple  $(C, \gamma)$  ( $(\tilde{C}, \tilde{\gamma})$ ), no one satisfies the inequality  $A \geq A_{lb}$  ( $RMSE \leq RMSE_{ub}$ ); in such a case, the value selected for  $A_{lb}$  ( $RMSE_{ub}$ ) has been reduced (increased) according to the simple mathematical law given below and the grid-search procedure has been repeated. In our computer simulations the following specific choices have been made for the grid-search method employed with PMs #2 and #3:

- The value  $A_{th}=75\%$  (90%) has been initially selected for class #1 (class #2) environments and, when needed, was reduced subtracting  $x_{step} = 5$  dBm ( $x_{step} = 5$  dBm) from it;
- The value  $RMSE_{ub} = 8$  dBm has been selected for both class #1 and class #2 environments and, when needed, the last value of  $RMSE_{ub}$  was replaced with the larger value  $\sqrt{RMSE_{ub}^2 + 4}$ ;
- The search interval for the optimal value of  $C$  ( $\tilde{C}$ ) has been restricted to  $[2^{-8}, 2^{10}]$  ( $[2^{-3}, 2^{10}]$ ), whereas that for the optimal value of  $\gamma$  ( $\tilde{\gamma}$ ) to  $[2^{-8}, 2^6]$  ( $[2^{-8}, 2^3]$ ).

These choices have originated from a trial and error method, whose starting point have been provided by some practical rules illustrated in [21] and [31].

### B. Performance results

Our software tool has been run for various areas belonging to class #1 and class #2. We have mainly focused on PM #3, because of its practical relevance. However, when operating according to this prediction mode, our classification and regression algorithms for each of considered areas have been trained using the measurements collected in all the other areas

of the same class (since a blind prediction was accomplished). The performance improvement that may originate from including in the training set of PM #3 the measurements acquired in the considered village/city, but not in the same district, has also been assessed; this modified version of PM #3 is denoted PM #3' in the following. Various performance results referring to the PMs #3 and #3' are shown in Table I and Table II for class #1 and class #2, respectively (in Table II Rocca Malatina A and Rocca Malatina B refer to the same area in the village of Rocca Malatina, but to different positions of the transmitter used in our measurement campaigns). From these results it is easily inferred that:

- A good accuracy (in particular, a limited RMSE) is achieved by our classification (regression) algorithm in most of the considered cases. Note that in the technical literature about path loss models for cellular communications at different frequencies it is commonly stated that, if measurements are fitted to standard path loss models in specific environments, a RMSE slightly larger than 9-10 dB can be achieved over a given link (e.g., see [34] and [35]). However, it is also known that the last approach has the following important drawback: the percentage of links over which each fitted model makes a reliable prediction is quite low (10-15%). Our results have evidenced that our approach does not suffer from this problem and that, in some cases, the RMSE is even below 9 dB.
- In various environments, the full-scale accuracy  $A_{fs}$  is not far from the accuracy  $A$ ; this means that the classification capability does not undergo a significant degradation as we approach the border of coverage area.
- The values of the parameter  $P_{fp}$  are limited in most of the considered scenarios.
- The geographical areas in which the worst results in terms of accuracy or RMSE are found with PM #3 (e.g., Concordia exhibits a small accuracy) are those significantly deviating, in terms of macroscopic characteristics of the propagation environment, from all the others areas included in the same class (i.e. class #1). For this reason, the classification and regression algorithms are trained by means of a data set that does not completely match with the considered environments.
- In some cases PM #3 performs slightly better than PM #3'; this derives from the fact that the exploitation of measurements collected in the same village/city which the considered environment belongs to does not necessarily improve accuracy, since distinct districts of such a village/city may exhibit substantially different propagation conditions.

Finally, further numerical results, not shown here for space limitations, have evidenced that, in various cases, the performance results obtained with PM #1 and PM #3 for the same area are very close. This leads to the conclusion that the SVMTRP is an efficient tool for radio planning and that, in particular, it can generate reliable blind predictions.

Radio planning area	PM #	$A$	$RMSE$	$A_{fs}$	$P_{fp}$
Bologna	3	82.26	7.70	82.19	17.47
Concordia	3	66.22	6.77	58.62	8.13
Modena	3'	90.80	7.53	91.36	16.16
Modena	3	91.03	13.44	94.20	30.11

TABLE I: Performance results for even areas (class #1).

Radio planning area	PM #	$A$	$RMSE$	$A_{fs}$	$P_{fp}$
Rocca Malatina A	3'	87.31	10.27	78.79	5.62
Rocca Malatina B	3'	81.79	9.75	84.57	20.98
Rocca Malatina A	3	87.94	9.93	80.96	6.73
Rocca Malatina B	3	82.04	10.45	89.14	23.62
Isera	3	83.30	9.08	86.85	21.40

TABLE II: Performance results for hilly/mountainous areas (class #2).

### C. Radio coverage estimation

In developing our SVMTRP, substantial attention has been also paid to its capability of generating useful graphical outputs for radio planning when PM #2 is employed. In the following we show some results referring to the village of Rocca Malatina, in which two data concentrators have been placed at specific locations (the coordinates and heights of these devices are listed in Table III); the area taken into consideration for radio planning and the geographical coordinates of the concentrators inside it are shown in Fig. 5. Note also that the RSS inside the considered area is estimated at the vertices of a square lattice, whose step size is equal to 8 m. The resulting outputs are shown in Figs. 7 and 8. In particular, Figs. 7a and 7b show the predicted RSS maps for the concentrator # 1 and concentrator # 2, respectively; note that these figures are both based on the chromatic scale shown in Fig. 6. Merging the data shown in Figs. 7a and 7b produces Fig. 7c, in which the colour selected for each point of the delimited area is associated with the strongest signal received from the two concentrators. The last graphical output is represented by Fig. 8, which shows, for each point of the delimited area, the best server (i.e., the transmitter providing the strongest received signal); in particular, the area covered by the blue (red) color is associated with concentrator #1 (#2).

## VI. CONCLUSIONS

In this manuscript SVM-based method for the planning of a radio network deployed for smart metering and operating

	Latitude	Longitude	Height
Concentrator # 1	44.389708°	10.965048°	3 m
Concentrator # 2	44.382775°	10.969014°	3 m
Vertex #1 (V1)	44.391575°	10.956505°	
Vertex #2 (V2)	44.377973°	10.973155°	

TABLE III: Geographic coordinates of the transmitters employed in our measurement campaigns in the Rocca Malatina area; the coordinates of two opposite vertices of the rectangular domain considered in our simulations for radio planning are also given.

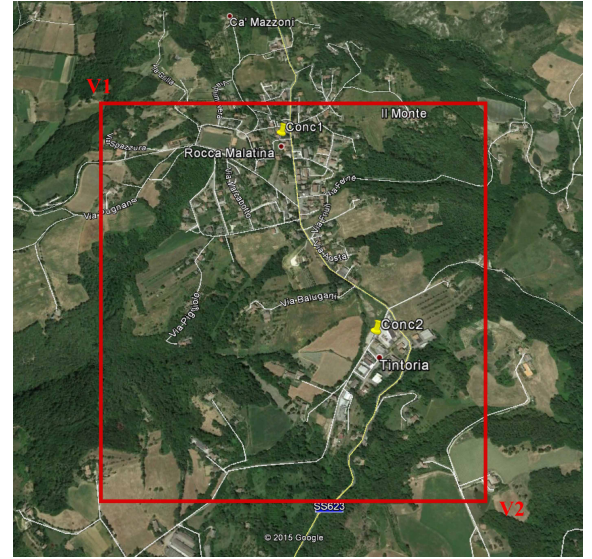


Fig. 5: Geographic area considered in our blind prediction of radio coverage in Rocca Malatina.

RSS Range (dBm)		Color
-109	-120	Grey
-106	-108	Purple
-103	-105	Blue
-100	-102	Cyan
-95	-99	Green
-90	-94	White
-80	-89	Yellow
-70	-79	Orange
-10	-69	Red

Fig. 6: Chromatic scale adopted in our signal strength maps.

in the 169 MHz band has been developed and its implementation in the MATLAB environment has been discussed. The efficacy of the devised method has been assessed in different geographical areas of northern Italy. Our results evidence that: a) our method achieves a good accuracy at the price of a moderate computational effort and exploiting a limited set of measurements; b) it is able to reliably predict the coverage area and the field strength map in environments for which RSS measurements are unavailable, but whose structure is similar to that of other environments for which such measurements have been already acquired. Our future research work will concern the exploitation of the proposed method for wireless network planning in other frequency bands.

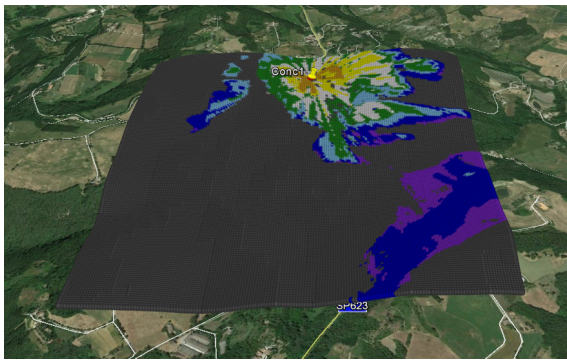
### ACKNOWLEDGMENT

We would like to thank Mr. Stefano Bianchi, Mr. Andrea Cavazzoni and Mr. Tiziano Zocchi (all from CPL Concordia) for their support and their constructive comments, and Mr. Nicola Tobia (from CPL Concordia too) for his comments and for his contribution to the development of the hardware tools employed in our measurements campaigns.

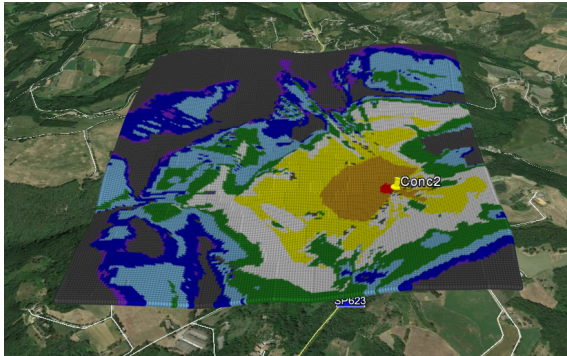
### REFERENCES

- [1] The OMS-Group, Norm EN 13757-4:2005: Communication systems for meters and remote reading of meters - Part 4: Wireless meter readout

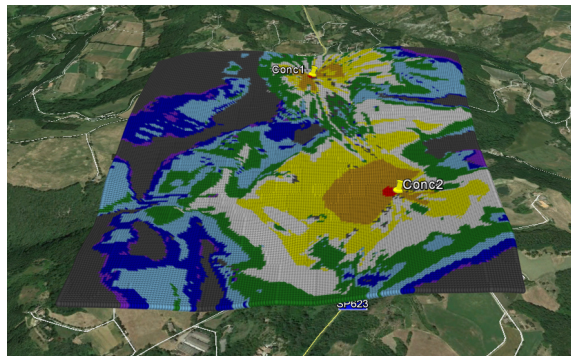




(a) Signal strength map for concentrator #1.



(b) Signal strength map for concentrator #2.



(c) Signal strength map for both concentrators. The colour selected for each point is associated with the strongest signal received from the two concentrators.

Fig. 7: Example of graphical outputs for PM #2; the Rocca Malatina village is considered.

(Radio meter reading for operation in the 868 MHz to 870 MHz SRD band), 2005.

- [2] The OMS-Group, Norm EN 13757-4:2011: Communication systems for meters and remote reading of meters - Part 4: Wireless meter readout (Radio meter reading for operation in SRD bands), 2013.
- [3] CEPT Electronic Communications Committee, ERC/REC 70-03, Relating to the Use of Short Range Devices (SRD), Oct. 2013.
- [4] F. Fuschini, M. Barbiroli, G. E. Corazza, V. Degli-Esposti and G. Falciassecca, "Analysis of Outdoor-to-Indoor Propagation at 169 MHz for Smart Metering Applications", *IEEE Trans. on Ant. and Prop.*, vol. 63, no. 4, pp.1811-1821, April 2015.
- [5] C. Phillips, D. Sicker and D. Grunwald, "A Survey of Wireless Path Loss Prediction and Coverage Mapping Methods", *IEEE Communications Surveys & Tutorials*, vol.15, no.1, pp.255-270, First Quarter 2013.
- [6] Y. Okumura, E. Ohmori, T. Kawano and K. Fukuda, "Field strength and its variability in VHF and UHF land mobile radio service", *Rev. Electr. Commun. Lab.*, vol. 16, pp. 825-873, 1968.
- [7] M. Hata, "Empirical Formula for Propagation Loss in Land Mobile

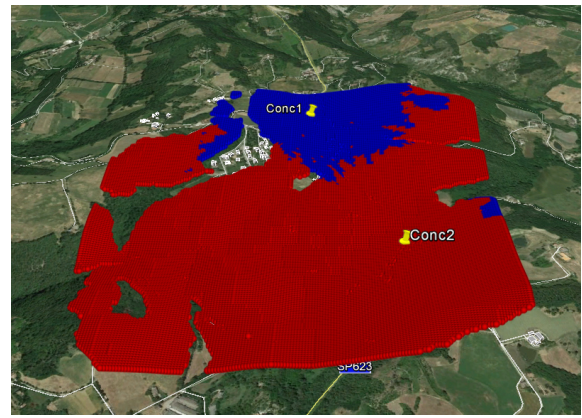


Fig. 8: Best server output in PM #2. The Rocca Malatina village is considered; concentrator #1 (#2) is represented by the blue (red) color. The absence of these colors in some parts of the considered area indicates that no useful signal is received from the two concentrators.

- Radio Services", *IEEE Trans. Veh. Tech.*, vol. 29, pp. 317-25, 1980.
- [8] T. Rautiainen, G. Wüölfle and R. Hoppe, "Verifying Path Loss and Delay Spread Predictions of a 3D Ray Tracing Propagation Model in Urban Environments", *Proc. of the 56th IEEE Veh. Tech. Conf. (VTC 2002 - Fall)*, Vancouver, Canada, Sept. 2002.
- [9] C. M. Bishop, **Pattern Recognition and Machine Learning**, Springer-Verlag, 2006.
- [10] F. Laganiço, M. Cacciola, S. Calcagno, D. De Carlo, G. Megali, M. Versaci and F. C. Morabito, "Evaluating Soft Computing Techniques for Path Loss Estimation in Urban Environments", *Proc. of the 2009 Conf. on Neural Nets (WIRN09)*, pp. 323-331, Salerno (Italy), May 28-30 2009.
- [11] Po-Rong Chang and Wen-Hao Yang, "Environment-adaptation mobile radio propagation prediction using radial basis function neural networks", *IEEE Trans. Veh. Tech.*, vol. 46, no. 1, pp.155-160, Feb 1997.
- [12] T. Balandier, A. Caminada, V. Lemoine and F. Alexandre, "170 MHz field strength prediction in urban environment using neural nets", *Proc. of the Sixth IEEE Int. Symp. on Personal, Indoor and Mobile Radio Commun. (PIMRC'95)*, vol. 1, pp.120-124, 27-29 Sep. 1995.
- [13] R. Fraile and N. Cardona, "Macrocellular coverage prediction for all ranges of antenna height using neural networks", *Proc. of the IEEE 1998 Int. Conf. on Universal Personal Commun. (ICUPC '98)*, vol. 1, pp.21-25, 5-9 Oct 1998.
- [14] I. Popescu, A. Kanstas, E. Angelou, I. Naformita and P. Constantinou, "Applications of generalized RBF-NN for path loss prediction", *Proc. of the 13th IEEE Int. Symp. on Personal, Indoor and Mobile Radio Commun. (PIMRC 2002)*, vol. 1, pp. 484-488, 15-18 Sept. 2002.
- [15] M. Kasparick, R. L. G. Cavalcante, S. Valentin. S. Stanczak and M. Yukawa, "Kernel-Based Adaptive Online Reconstruction of Coverage Maps with Side Information", available at <http://arxiv.org/pdf/1404.0979.pdf> Apr. 2014
- [16] M. Piacentini and F. Rinaldi, "Path loss prediction in urban environment using learning machines and dimensionality reduction techniques", *Computational Management Science*, vol. 8, no. 4, pp. 371-385, March, 2010.
- [17] G. Durgin, T. S. Rappaport and Hao Xu, "Measurements and models for radio path loss and penetration loss in and around homes and trees at 5.85 GHz", *IEEE Trans. Commun.*, vol. 46, no. 11, pp. 1484-1496, Nov. 1998.
- [18] Robson D. A. Timoteo, Daniel C. Cunha, George D. C. Cavalcanti, "A Proposal for Path Loss Prediction in Urban Environments using Support Vector Regression", *Proc. of the Tenth Advanced Int. Conf. on Telecommun. (AICT 2014)*, pp. 119-124.
- [19] C. Cortes and V. Vapnik, "Support-Vector Networks", *Machine Learning*, vol. 20, no. 3, pp. 273-297, Sep. 1995.
- [20] B. E. Boser, I. M. Guyonand V. N. Vapnik, "A training algorithm for optimal margin classifiers", *Proc. of the fifth annual workshop on Comput. learning theory (COLT '92)*, ACM, New York (NY), USA, pp. 144-152, 1992.
- [21] Chih-Wei Hsu, Chih-Chung Chang, and Chih-Jen Lin, "A

- practical guide to support vector classification”, available at <http://www.csie.ntu.edu.tw/~cjlin/papers/guide/guide.pdf>
- [22] C. J. C. Burges, “A Tutorial on Support Vector Machines for Pattern Recognition” [research.microsoft.com/pubs/67119/svmtutorial.pdf](http://research.microsoft.com/pubs/67119/svmtutorial.pdf).
  - [23] V. Vapnik, **Statistical Learning Theory**. John Wiley and Sons, Inc., New York, 1998.
  - [24] Meter Italia, “EG-4 residential natural gas smart meter with remote communication and management system”, available at <http://www.meteritalia.com/wp-content/uploads/2014/06/EG-4.pdf>.
  - [25] Radiocrafts, “RC1701xx-MBUS - Wireless M-Bus High power N Mode RF Transceiver Module EN 13757-4:20130”, available at [http://www.radiocrafts.com/uploads/rc1701xx-mbus\\_datasheet\\_1\\_11.pdf](http://www.radiocrafts.com/uploads/rc1701xx-mbus_datasheet_1_11.pdf).
  - [26] Sirio antenne, “SKB 108-960 - Installation manual”, available at [http://www.sirioantenne.it/product-manual/Id-378\\_379.pdf](http://www.sirioantenne.it/product-manual/Id-378_379.pdf).
  - [27] GeoShack, “AM50 - Product brochure”, available at <http://geoshack.com/am50>.
  - [28] T. Vincenty, **Direct and inverse solutions of geodesics on the ellipsoid with application of nested equations**. *Survey Review*, 22(176):88–93, 1975.
  - [29] QGIS, “A Free and Open Source Geographic Information System”, available at <http://www.qgis.org>.
  - [30] MATLAB, “Mapping Toolbox”, available at <http://www.mathworks.com/products/mapping>.
  - [31] Chih-Chung Chang, and Chih-Jen Lin, “LIBSVM - A Library for Support Vector Machines”, available at <http://www.csie.ntu.edu.tw/~cjlin/libsvm/>
  - [32] Geoportal of Emilia Romagna, available at <http://geoportale.regione.emilia-romagna.it/it/download/databasetopografico>.
  - [33] Geoportal of the autonomous province of Trento, available at <http://www.territorio.provincia.tn.it>.
  - [34] J. N. C. de Oliveira, M. S. Alencar, V. C. da Rocha, W. T. A. Lopes, “A new propagation model for cellular planning”, *Proc. of the 2006 Int. Telecommun. Symp.*, pp. 35-37, 3-6 Sept. 2006
  - [35] C. Phillips, D. Sicker and D. Grunwald, “Bounding the error of path loss models”, *Proc. of the IEEE Symp. on New Frontiers in Dynamic Spectrum*, April 2011.